Geosci. Model Dev. Discuss., 6, 4883–4932, 2013
www.geosci-model-dev-discuss.net/6/4883/2013/
doi:10.5194/gmdd-6-4883-2013

Geoscientific Model Development
Discussions
Open Access

Modeling different freeze/thaw processes in heterogeneous landscapes of the Arctic polygonal tundra using an ecosystem model

S. Yi[1,2], K. Wischnewski[2], M. Langer[2], S. Muster[2], and J. Boike[2]

[1]State Key Laboratory of Cryospheric Sciences, Cold and Arid Regions Environmental and Engineering Research Institute, 320 Donggang West Road, 730000, Lanzhou, Gansu, China
[2]Alfred Wegener Institute for Polar and Marine Research, Telegrafenberg A43, 14473 Potsdam, Germany

Received: 4 June 2013 – Accepted: 3 September 2013 – Published: 16 September 2013

Correspondence to: S. Yi (yis@lzb.ac.cn)

Published by Copernicus Publications on behalf of the European Geosciences Union.

Abstract

Freeze/thaw (F/T) processes can be quite different under the various land surface types found in the heterogeneous polygonal tundra of the Arctic. Proper simulation of these different processes is essential for accurate prediction of the release of greenhouse gases under a warming climate scenario. In this study we have modified the dynamic organic soil version of the Terrestrial Ecosystem Model (DOS-TEM) to simulate F/T processes beneath the polygon rims, polygon centers (with and without water), and lakes that are common features in Arctic lowland regions. We first verified the F/T algorithm in the DOS-TEM against analytical solutions, and then compared the results with in situ measurements from Samoylov Island, Siberia. In the final stage, we examined the different responses of the F/T processes for different water levels at the various land surface types. The simulations revealed that (1) the DOS-TEM was very efficient and its results compared very well with analytical solutions for idealized cases, (2) the simulations compared reasonably well with in situ measurements although there were a number of model limitations and uncertainties, (3) the DOS-TEM was able to successfully simulate the differences in F/T dynamics under different land surface types, and (4) permafrost beneath water bodies was found to respond highly sensitive to changes in water depths between 1 and 2 m. Our results indicate that water is very important in the thermal processes simulated by the DOS-TEM; the heterogeneous nature of the landscape and different water depths therefore need to be taken into account when simulating methane emission responses to a warming climate.

1 Introduction

The release of greenhouse gases from the large quantities of soil carbon preserved in Arctic regions constitutes an important feedback to climatic warming and the thawing of permafrost north of 45° N (McGuire et al., 2009; von Deimling et al., 2012). Reliable simulation of the dynamics of permafrost is therefore critical when predicting future climatic changes. The energy balance of ground surface has an important influence on variations in permafrost. Heterogeneous ground surfaces with, e.g., variable snow pack thicknesses and organic layer thicknesses, have a large influence the on surface energy balance (Etzelmüller and Frauenfeld, 2009), and have in the past been integrated into both land surface models (Yi et al., 2007; Lawrence and Slater, 2008) and ecosystem models (Zhuang et al., 2001; Yi et al., 2009a, b, 2010). Water bodies of various sizes, ranging from those occupying polygon centers to large thermokarst lakes, are distributed across the Arctic coastal regions (French, 2007) resulting in considerable landscape heterogeneity. Water bodies strongly affect the surface energy balance and the thermal dynamics of the surrounding permafrost soils (French, 2007). Their presence can lead to permafrost degradation which in turn affects the terrestrial ecosystem carbon budget. For example, outgassing of carbon dioxide from ponds and lakes was found to account for between 74 and 81 % of the calculated net landscape-scale CO_2 emissions during September (Abnizova et al., 2012). However, few of the current large scale land surface models or ecosystem models take into account the effects that water bodies have on the dynamics of permafrost (Zhuang et al., 2006; Ringeval et al., 2012), with one exception being the model by Wania et al. (2009) which treated surface water in the same way as a litter layer.

There are a number of different techniques for simulating permafrost dynamics (Riseborough et al., 2008). A wide range of numerical models exist which are applied in both standalone permafrost simulations and land-surface schemes of climate models. Soil temperatures and water content at different depths of soil or rock are calculated numerically. In large scale models numerical solutions of permafrost dynamics are commonly obtained by solving finite difference equations. One category of numerical solution, referred to by Zhang et al. (2008) as ”decoupled energy conservation parameterization”, assumes that the soil water is homogeneous and freezes or thaws at exactly 0 °C; if following calculation of the soil temperature for each layer the temperature of a particular layer that contains ice is greater than 0 °C, some or all of the ice will melt and the temperature is then recalculated, and *vice versa*. This is an efficient method and is

GMDD
6, 4883–4932, 2013

commonly used in land surface models (Zhang et al., 2003; Oleson et al., 2004). However, the lower layers in land surface models are usually thick and the derived freezing or thawing fronts from soil temperature interpolation are not realistic (Yi et al., 2006).

A second category of numerical methods, referred to by Zhang et al. (2008) as "apparent heat capacity parameterization", assumes that soil water freezes or thaws over a range of temperatures below 0 °C and simulates the unfrozen soil water content and temperature simultaneously. Since small changes of soil temperature in the freeze/thaw range will result in a large change in apparent heat capacity, an iterative procedure is required to ensure small changes of temperature at each time interval (Nicolsky et al., 2007). This method is commonly applied in permafrost models (Goodrich, 1978; Nicolsky et al., 2007; Dall' Amicoet al., 2011; Hipp et al., 2012; Langer et al., 2013) and has also recently been applied in a land surface model (Ringeval et al., 2012). Although the method is more physically realistic it requires greater computing resources. This may lead to limitations in spatial resolution, length of time that can be modeled, and number of simulated land surface classes, etc.

Both categories of numerical models have their disadvantages when they are applied for regional permafrost simulation. Besides numerical models, analytical solutions also exist for solving phase change problems. For example, exact Neumann solutions to freezing and thawing problems exist for idealized cases, e.g. for infinite or semi-infinite homogeneous material, steady upper boundary conditions, etc. (Lunardini, 1981). Stefan's equation, which was originally used to predict the thickness of sea ice, is widely used due to its simple form (Lunardini, 1981); an algorithm for applying Stefan's equation to a layered system (e.g. soil) was developed by Jumikis (1977) and applied in a hydrological model by Fox (1992). However, predictions from the Stefan algorithm usually overestimate the depths of freeze/thaw fronts as heat transport below front is neglected. In order to mitigate this problem of overestimation, Woo et al. (2004) developed a two-directional Stefan algorithm (TDSA). Yi et al. (2009a) integrated a TDSA within a Terrestrial Ecosystem Model (TEM) in order to first simulate the depths of freezing or thawing fronts and then update the soil temperatures for layers above the uppermost front, below the lower most front, and between these two fronts. This is an efficient method and is able to track the positions of fronts within thick soil layers.

Although models using the above methods to simulate permafrost dynamics over large regions have been validated using in situ measurements, few of them have been verified against analytical solutions for both freezing and thawing fronts and soil temperatures at different depths, which is as important as model validation (Romanovsky et al., 1997).

In this study we aimed to develop and test a model that could simulate permafrost dynamics under different types of land surface, i.e. different thicknesses of snow cover, of the organic layer, and of water. We first verified our dynamic organic soil version of the TEM (DOS-TEM) with analytical solutions for idealized cases; we then modified the model to take into account the effects that water bodies of various sizes have on the thermal dynamics of permaforst and compared the output with in situ measurements from Samoylov Island, Siberia. Finally, we compared the simulations under different land surface types in order to investigate the vulnerabilities of permaforst to water bodies.

2 Methods

2.1 Site description

Samoylov Island (72° 22′ N, 126° 30′ E) is located in the southern-central part of the Lena River Delta of Siberia (Fig. 1); it covers an area of about 7.5 km^2. The average annual mean air temperature on Samoylov Island from 1998–2011 was −12.5 °C and the average total summer rainfall 125 mm (Boike et al., 2013). Samoylov Island contains two major geomorphological units: a floodplain, and an elevated Holocene terrace which is characterized by low-centered polygonal tundra. The elevated terrace comprises ∼70 % of the total area of the island and contains numerous ponds and thermokarst lakes. On average, the land surface of the terrace consists of 58 % dry

GMDD
6, 4883–4932, 2013

tundra, 17 % wet tundra, and 25 % water surfaces (Muster et al., 2012). Further information concerning the climate, permafrost, vegetation, and soil characteristics can be found in Boike et al. (2013).

Meteorological data processing

The collection of meteorological measurements on Samoylov Island started in 1998. The daily mean air temperature, wind speed, vapor pressure, net radiation, downward solar radiation, and total daily precipitation were calculated from hourly measurements. If more than 25 % of the measurements were missing in any one day, no value was recorded for that day. If more than 25 % of the daily values in a particular month were missing, no value was recorded for that month. We replaced the missing monthly values as follows:

1. Air temperature and precipitation (snow + rain) measurements for the same month, available from the nearby Stolb meteorological station (which has datasets from 1956, but with large gaps during the 1970s), were used to replace the missing values.

2. Long term-mean values were used to replace some values for air temperature and precipitation that remained missing after step (1) above, as well as missing values for wind speed, radiation, and vapor pressure. We calculated the long-term monthly mean for air temperature and precipitation between 1981 and 2011 using measurements from the Stolb meteorological station, and for wind speed, downward shortwave radiation, and vapor pressure between 1998 and 2011 using measurements from the Samoylov site;

To illustrate the differences between different datasets, we compared the monthly air temperature and precipitation datasets from Samoylov Island with those from Stolb and the global reanalysis dataset from the Climate Research Unit (CRU TS3.1) available from http://badc.nerc.ac.uk/view/badc.nerc.ac.uk__ATOM__dataent_1256223773328276 (Fig. 2).

2.2 Model descriptions

The Terrestrial Ecosystem Model (TEM) family of models is designed to simulate the carbon and nitrogen pools within vegetation and soil, and the carbon and nitrogen fluxes between vegetation, soil, and the atmosphere (McGuire et al., 1992). The most recent TEM version (i.e. the DOS-TEM) can simulate the dynamics of organic soil layers, which can be subject to fire disturbances and to ecological successions (Yi et al., 2010). The DOS-TEM consists of four modules, these being the environmental, ecological, fire disturbance, and dynamic organic soil modules. The environmental module operates on a daily time interval using mean daily air temperature, surface solar radiation, precipitation, and vapor pressure, which are downscaled from monthly input data (Yi et al., 2009a). It takes into account radiation and water fluxes between the atmosphere, canopy, snow pack, and soil. Soil moisture and temperature of all soil layers are updated daily. A two-directional Stefan algorithm is used to predict the depths of freezing or thawing fronts within the soil (Woo et al., 2004); it first simulates the depth of the front in the soil column from the top downward, using soil surface temperature as the driving temperature; it then simulates the front from the bottom upward using the soil temperature at a specified depth beneath a front as the driving temperature (bottom-up forcing). If a layer contains a freezing or thawing front, this layer is then divided into two layers (Figure A1b). The temperatures of soil layers above the uppermost freezing or thawing front and below the lowermost freezing or thawing front are updated separately by solving finite difference equations. The thermal properties of soil layers are affected by their water content (Yi et al., 2009a).

2.3 Model modifications

We made three modifications to the DOS-TEM in order to simulate the effects that water bodies (Fig. A1a) have on freezing or thawing processes. (1) We took into account the effect of the soil surrounding water bodies by calculating the volumetric water content of different layers within water bodies of various sizes (Fig. A2); details are presented

GMDD
6, 4883–4932, 2013

in Appendix A. (2) When updating the thermal state of water layers they were treated in the same way as soil layers, but with different thermal properties. We followed the model of Hostetler et al. (1990) to calculate the eddy diffusion coefficients for the water layers, which were then used together with the molecular diffusion coefficient of water to calculate the heat transfer within the water bodies and the heat exchange with the underlying sediments. Details are presented in Appendix B. (3) The original DOS-TEM only simulated bottom-up forcing for the deepest freezing or thawing front. However, taliks probably exist beneath some water bodies, and more than 2 freezing or thawing fronts may exist at the same time. We therefore implemented bottom-up forcing separately for each front (Fig. A1b).

The soil thermal conductivity in the DOS-TEM was initially calculated according to Farouki (1986). However, preliminary testing showed that the calculated soil thermal conductivities were higher than those derived from field measurements (Langer, et al., 2011). Hence, in this study we used the more realistic parameterization according to Johansen (1975) and Côté and Konrad (2005). More details on the used parameterization are provided in Appendix B.

2.4 Model verification, validation and sensitivity tests

2.4.1 Comparisons with analytical solutions

Three different materials were tested in this study, i.e. water, mineral (sand), and organic soil. The properties of these materials are listed in Table 1. The initial temperature of each material at different depths (up to 5000 m in the DOS-TEM) was set to −10 °C, the temperature at upper boundary was set to 5 °C over the whole simulation period (100 yr). We assumed zero heat flux condition at the lower boundary in 5000 m depth. The temperatures and the depth of the thawing front obtained from the DOS-TEM were compared with those from analytical solutions and those obtained using the one-directional Stefan's equation. For the DOS-TEM, the temperature at a specific depth was calculated by linear interpolation between the temperatures of upper and lower layers. To test the sensitivity of the model to the depth used for the bottom-up forcing, we tried bottom-up forcing at different depths below the thawing front (i.e. 50 cm, 1, 2, 5, and 20 mbelow). In order to test the effects of total soil/water thickness, we also evaluated the DOS-TEM for different depths of lower boundary (50, 500 and 5000 m). The maximal thicknesses of the soil/water layer were 1, 10, and 100 m for the runs with the lower boundary located in 50, 500, and 5000 m depth so that the total number of layers was constant for each run.

2.4.2 Comparisons with in situ measurements

Test sites

We tested the DOS-TEM for soil or water temperatures at 4 different sites, i.e. on a polygon rim (*rim*), in a polygon center without standing water (*center*), in a polygon center with standing water (*pond*), and at larger thermokarst lake (*lake*). These sites are considered to represent the most prominent types of land surfaces in the polygonal tundra landscape of Samoylov Island. The configuration of the water and organic soil characteristics for the different land surface types used in the model are presented in Table 2. We used about 65 m of mineral soils (saturated sand with a porosity of 0.6) in 12 layers. The DOS-TEM assumes bedrock beneath the soil layer (Fig. A1a); in each case we used 420 m of bedrock in 5 layers to represent the frozen sediments on Samoylov Island. The ground heat flux at the bottom of the bedrock was set to 0.053 w/m^2 (Pollack et al., 1993).

The simulated soil temperatures at the four different land surface types were compared to temperature measurements from a 27 m borehole on Samoylov Island (Boike et al., 2013).

GMDD
6, 4883–4932, 2013

Surface temperatures

The DOS-TEM does not simulate the surface temperatures of water, land, or snow. We therefore established the relationships between measured daily surface temperatures and air temperatures in 2011 as follows: for water $T_{surf} = 0.563\ T_{air} + 4.735$ (coefficient of determination $R^2 = 0.41$, number of pairs of data $n = 84$), for land, $T_{surf} = 0.643\ T_{air} + 2.231$ ($R^2 = 0.54$, $n = 84$), and for snow we assumed $T_{surf} = T_{air}$.

Snow

Wind drift is an important process that redistributes snow in the polygonal tundra landscape. Field measurements of annual maximum snow thickness are usually 15–40 cm in polygon centers and much less on polygon rims and frozen lakes (Boike et al., 2013). Zhang et al. (2012) introduced a snow drift factor in their NEST model. The factors for polygon rims, polygon centers without standing water, and polygon centers with standing water are 0.5, 0, and −0.25, respectively, with a positive value indicating a loss of snow due to wind drift. However, a preliminary model run indicated that the simulated snow thicknesses were overestimated for all sites. Therefore the maximum snow thickness was set to 0.1 m for both polygon rims and lakes. For polygon centers we assumed that

$$D_{snw,\,max} = (WD_{max} - WD) + 0.1 \tag{1}$$

where $D_{snw,\,max}$ is the maximum snow thickness (m), WD_{max} is the maximum water depth (m), and "WD" is the actual water depth (m) (see Fig. A2).

We also assumed that snow only accumulates when the top layer of the soil or water is frozen.

GMDD
6, 4883–4932, 2013

Soil and water properties

For the soil thermal properties we used two sets of parameters, one derived from field temperature measurements (Langer et al., 2011) and the other calculated from an algorithm proposed by Luo et al. (2009), details of which can be found in Appendix B (Table 3). For water, we increased the calculated value of the eddy diffusion coefficient by a factor of between 10 and 100 following Subin et al. (2012), in order to take into account the effects of convection currents caused by complex lake topography and density instability.

Initialization

The *rim*, *center*, and *pond* sites were all initialized using a temperature of $-10\,^{\circ}\mathrm{C}$ for all water, soil, and bedrock layers; the *lake* site was initiated with $-10\,^{\circ}\mathrm{C}$ for all soil and bedrock layers and with $0\,^{\circ}\mathrm{C}$ for water layers. In order to reach realistic temperature distributions within the ground, the model was run to a dynamic equilibrium over a 100 year period at the rim, center, and pond sites and a 200 yr period at the lake site. For the equilibrium run, the model was forced by an average annual cycle that was generated from the monthly averages of the available climate data from 1981–2011. The state of equilibrium was verified by additional runs using longer periods of 400 and 600 yr, respectively. The period from 1981–2003 was used for model spin-up, and we compared the simulations with measurements collected after 2003.

2.4.3 Effects of (maximum) water depth

Polygon centers and lakes of various sizes and water depths are distributed across much of Samoylov Island. In order to investigate the effect that the size and water depth of polygon ponds and lakes have on the thickness of unfrozen soil underneath, we ran the DOS-TEM for a shallow, medium, and deep polygon pond (with maximum water depths of 20, 60, and 120 cm), and for a shallow, medium, and deep lake (with

GMDD
6, 4883–4932, 2013

maximum water depths of 3, 6, and 9 m). For each polygon pond or lake the model was run with no water (empty), with 50 % (half full), and 100 % (full) of the maximum water depth. The annual mean unfrozen soil thickness from 1981 to 2011 was calculated for comparison.

3 Results

3.1 Comparisons with exact Neumann solutions and Stefan equations

The bottom-up forcing in the DOS-TEM is very important for accurate simulation of the position of the thawing front using Stefan's algorithm (Fig. 3). For all cases of water, mineral soil, and organic soil the thawing fronts simulated without bottom-up forcing were very close to those calculated using Stefan's equation. The root mean squared errors (RMSEs, $n = 36\,500$) between simulated thawing fronts without bottom-up forcing and those from exact Neumann solutions for three different idealized cases were greater than 1.128 m. In contrast, the RMSEs between the simulated thawing fronts with bottom-up forcing and those from exact Neumann solutions were less than 0.047 m (Table 4).

The simulated water or soil temperatures and thawing fronts were not sensitive to the depth of bottom-up forcing (Fig. 3). For example, there were almost no differences in the simulated thawing fronts for bottom-up forcing at depths from 0.5–20 m in all three cases. The differences between simulations of the thawing front using these bottom-up forcing and Neumann solutions were also very small (Fig. 3). Taking bottom-up forcing at 1 m beneath the thawing front as an example, most of the RMSEs for temperatures at depths shallower than 1 m were less than 0.01 °C, and 0.1 °C for depths greater than 1m (Fig. 4 and Table 5).

The simulated temperatures are sensitive to the total thicknesses of the various materials, especially for mineral soil which has the highest thermal conductivity and the lowest water content (Table 4).

GMDD
6, 4883–4932, 2013

3.2 Comparisons with in situ measurements

3.2.1 Snow thicknesses

The simulated snow thickness from the DOS-TEM was more than 80 cm at all sites for 2005–2006, and decreased thereafter (Fig. 5). However, measurements at the center site showed that the monthly maximum snow thickness was only 40 cm. After setting a maximum snow thickness, the differences in snow thickness between the 4 sites were similar to field observations, but the inter-annual variability was very small. Since we assumed that snow only accumulates on frozen layers of water or soil, the starting date for snow accumulation at pond and lake sites was usually later than at rim and center sites. The simulated starting dates for snow accumulation in the autumn of 2010 were about one month later than the observed starting dates.

3.2.2 Temperatures of shallow layers

For the rim site, soil temperatures for model runs that included snow drift compared well with actual measurements at depths of both 2 cm and 51 cm. (Fig. 6). The simulated soil temperatures at 51 cm were slightly underestimated during summer months. The simulated soil temperatures using the calculated thermal properties (Appendix B) were close to those simulated using the derived thermal properties at 2 cm depth but varied by about 1–3 °C at 51 cm depth. The effect of snow was very obvious: where no maximum snow thickness had been set the simulated soil temperatures were up to 10 °C warmer than the measured soil temperatures.

For the center site, the performance of the DOS-TEM was similar to the rim site during the summer seasons (Fig. 7). The DOS-TEM overestimated the soil temperatures at 40 cm depth in several of the winters. Using different soil thermal properties did not result in any obvious differences in soil temperatures, and setting a maximum snow thickness had less effect than for the rim site.

For both rim and center sites, the simulated soil temperatures fell rapidly during the fall of 2010, possibly due to the later snow fall in the simulation (Figs. 5, 6 and 7).

For the pond site, the model underestimated water temperatures in summer and overestimated them in winter (Fig. 8). For example, the simulated water temperature in the lower part of the pond site was 20 °C warmer than actual measurements from the winter of 2008–2009. As an additional experiment we reduced the maximum snow thickness from 15–2 cm, which brought the simulated water temperatures in winter down to the measured temperatures. Setting a maximum snow thickness thus reduced the simulated water temperature in winter. Changing the water eddy diffusion coefficient by a factor of between 10 and 100 did not result in any obvious differences between model runs.

For the lake site, the simulated water temperatures in the upper part of the lake were not as sensitive to the eddy diffusion coefficient as those in the lower part of the lake (Fig. 9). The simulation using the default water eddy diffusion coefficient considerably underestimated the water temperature (by about 10 °C) in the lower part of the lake. Increasing the eddy diffusion coefficient by a factor of 100 improved the simulation.

In the following two subsections we only analyze the freezing and thawing fronts and the deeper soil temperatures on the basis of simulations with a maximum snow thickness, derived soil thermal properties, and an eddy diffusion coefficient increased by a factor of 100.

3.2.3 Freezing and thawing fronts

The simulated shapes of freezing and thawing fronts at the rim and center sites were similar from 2003 to 2011 (Fig. 10). The thawing fronts did not survive through the winter months and into the following year. However, the simulated thawing fronts at the pond site were usually static in summer and autumn, and usually extended through the winter into the following spring. In an additional test performed with 2 cm maximum snow thickness, the soil temperature was colder than it was with 15 cm maximum snow thickness and the shapes of the thawing fronts were different (Figs. 10, 3 and 4). However, from 2003 to 2011 the average maximum depth of thawing fronts in soils under water was 0.47 for simulations with 2 cm maximum snow thicknesses and 0.58 m for those with 15 cm maximum snow thickness. The simulated thawing fronts at the lake site occurred at an average depth of 9.67 m below the lake floor. We also performed an additional simulation using bottom-up forcing only for the deepest thawing front. Results showed only a few centimeters difference between the depths of freezing fronts in lake water from this additional simulation and those from the original simulation (details not included).

The maximum active layer thickness, which is defined as the maximum unfrozen thickness of the active layer over a complete year, varied in 2010 from 0.33 m in 2004 to 0.65 m at the rim site, from 0.34 m in 2004 to 0.57 m at the center site, and from 0.5–0.8 m below the floor of the polygon c pond. The DOS-TEM did not simulate any talik for these three sites between 2003 and 2011 but simulated about 9.67 m of talik beneath the lake site.

Increasing the equilibrium run time for the lake site, from 200 years to 400 or 600 yr increased the multi-year mean talik thickness between 2007 and 2011 from 9.67–1.46 or 13.60 m, respectively. Hence, no thermal equilibrium was reached at the lake site.

3.2.4 Temperatures of deep layers

The averages of the modeled annual mean soil temperatures at 26.75 m depth over the period from 2007–2011 were approximately −10.9, −9.2, −3.0, and −1.2 °C for the rim, center, pond, and lake sites, respectively (Fig. 11). The temperature at the same depth over the same period in the borehole was −8.8 °C. Only the modeled soil temperature profile for thecenter site was close to the borehole measurements. If the temperatures from the rim, center, and pond sites were averaged taking into account the proportions of dry tundra (58 %), wet tundra (17 %), and surface water (25 %) following Muster et al. (2012), the overall mean temperature would be −8.7 °C.

GMDD
6, 4883–4932, 2013

Increasing the equilibrium run time for the lake site from 200–400 or 600 yr increased the multi-year mean soil temperature at a depth of 26.75 m between 2007 and 2011 from −1.2 °C to −0.8 or −0.55 °C, respectively.

3.3 Effects of (maximum) water depth

For polygon centers, increasing either the water depth or the maximum water depth increased the annual mean unfrozen soil thickness (Fig. 12). Increasing the water depth in the lake also increased the unfrozen sediment thickness; the sensitivity of the unfrozen sediment thickness was particularly high when water depths were between 1 and 2 m; and very low when the water depth was greater than 2 m.

4 Discussion

4.1 Performance of the DOS-TEM

The simulated thawing fronts and soil/water temperatures at different depths compared very well with analytical Neumann solutions for all three materials, and the accuracy was not sensitive to the depth of bottom-up forcing (Figs. 3 and 4). The simulated soil/water temperatures compared reasonably well with in situ measurements from Samoylov Island in the Lena Delta, Siberia (Figs. 6, 7, 8, and 9).

The parameterization used to calculate soil/water temperatures in the DOS-TEM is very efficient. For example, it takes about 10 s for the DOS-TEM to simulate a period of 100 yr but it takes more than 30 min for a numerical model with apparent heat capacity parameterization to simulate a period of only 10 yr on same computer.

4.2 Effects of snow

Snow thickness has a strong impact on the soil/water temperatures during cold seasons. At the rim site, differences between simulated soil temperatures with and without taking snow drift into account were usually greater than 10 °C (Fig. 6). At the center site, the simulated snow thickness was greater than the measured thickness (Fig. 5) and the simulated soil temperatures were warmer than the measured temperatures (Fig. 7). The differences at the pond site were even greater (Fig. 8).

The timing of snowfall is an additional factor affecting the thermal dynamics of soils. The snowfalls simulated for the fall of 2010 were later than the measured snowfalls (Fig. 5), which caused early decreases in soil temperatures at the rim and center sites (Figs. 6 and 7). In the real world early snowfall might be expected to melt in the unfrozen water of the pond and lake sites; in the modeling, snow accumulated only after the first 2 cm of water was frozen. In the fall of 2010 there was therefore no time-lag between the simulated and measured water temperatures (Figs. 8 and 9).

4.3 Effects of water

Water ponding has a very important influence on the underlying unfrozen soil thickness (Fig. 10) and the permafrost temperature (Fig. 11). Under the present climate on Samoylov Island our sensitivity tests indicate that the unfrozen soil thickness is very sensitive to water depths of between 1 and 2 m. This has significant implications for the development of talik under thermokarst lakes: following the melting of segregated ice under polygonal tundra and associated surface subsidence the development of a thermokarst lake could accelerate if the water depth in the lake exceeds a certain threshold. Similarly, talik beneath a thermokarst lake could disappear if the water depth in the lake falls below a certain threshold (van Huissteden et al., 2011).

4.4 Outlook

Land surface is heterogeneous at various spatial scales and land surface models (LSMs) with coarse resolutions (usually hundreds of kilometers) take into account heterogeneity using different technologies. Early LSMs only considered the major land surface type within each grid cell (Manabe, 1969); parameters of different land surface types were subsequently aggregated for each grid (Arain et al., 1999). With recent advances in computing power and remote sensing technology, it has become possible to explicitly considered different types of land surface, such as those with different plant function types, urban areas, water, etc. (Oleson et al., 2004). Our study has indicated that the heterogeneity of Arctic polygonal tundra results in marked differences in soil thermal dynamics. In order to simulate methane emissions from polygonal tundra ecosystems on a regional scale it is therefore crucial to distinguish polygon rims, polygon centers (with varying water levels), and thermokarst lakes at different stages of development. The sensitivity analysis suggests that it is at least necessary to consider polygon rims, polygon centers with maximum water depths of less than 1.2 m, and lakes with water depths of both less than 2 m and greater than 2 m. The following steps can be taken to obtain regional input for the above-mentioned classes:

1. The proportion of surface water over regions of polygonal tundra ecosystem can be retrieved from remote sensing albedo datasets (Muster et al., 2013) and the maximal proportion of surface water over different periods calculated;

2. The distribution of the area covered by polygon centers can be established following Cresto Aleina et al. (2012);

3. The relationship between water area and water depth can be established on the basis of in situ measurement data (Wischnewski, 2013).

Few measurements of talik thickness beneath thermokarst lakes are available at present. This information is vital for determining the initial conditions and for validating model outputs. For example, it took less than 100 yr for the DOS-TEM to reach equilibrium at the rim and center sites but it did not reach equilibrium at the lake site, even after 600 yr. A new technology known as surface nuclear magnetic resonance, has recently been used over thermokarst lakes to measure talik thickness (Parsekian et al., 2013). This method promises to provide useful information on talik that can be used to improve modeling in future studies.

4.5 Limitations and uncertainties

Due to the harsh Arctic environment, some measurements of atmospheric variables are not available from Samoylov Island and the missing values were replaced with those from the nearby Stolb meteorological station. Air temperatures from the Stolb station (T_{stolb}) compared very well with those from Samoylov Island ($T_{samoylov}$): $T_{stolb} = 0.97\ T_{samoylov} + 0.65$; $R^2 = 0.99$; $n = 80$. The growing season precipitation at the Stolb station (P_{stolb}) also compared reasonably well with that for Samoylov Island ($P_{stolb} = 0.62\ P_{samoylov} + 8.35$; $R^2 = 0.53$; $n = 37$), with averages of 26.4 and 29.3 mm month^{-1}, respectively. Since there were no precipitation measurements for the cold seasons on Samoylov Island, it is impossible to assess any uncertainty associated with snowfall.

Running ecosystem models for regional or global applications requires large scale reanalysis datasets, such as the global datasets from the Climate Research Unit (CRU), the European Centre for Medium-Range Weather Forecasts (ECMWF), or the National Center for Environmental Prediction-National Center for Atmospheric Research (NCEP-NCAR). In this study, we compared the air temperature and precipitation from the CRU dataset with those from Samoylov Island. Air temperatures from the CRU were close to those for Samoylov Island in summer, but about 15 °C colder in January (Fig. 2). The monthly average precipitation in the growing season between 1998 and 2009 was 41.2 mm month^{-1} from the CRU and 29.3 mm month^{-1} for Samoylov Island. It is clearly important to investigate the uncertainties associated with input data when using models for large scale cold region applications (Clein et al., 2007).

Wind drift is a common process involved in redistributing snow on the heterogeneous landscape of the Arctic tundra (Sturm et al., 2001). There are, however, no measurements of snowfall and snow cover thickness available for the various terrain units of Samoylov Island, making the parameterization of snow drift impossible. Zhang et al. (2012) used snow drift factors and in this study we have set maximal snow thicknesses to simulate the differences in snow thicknesses between different land surface types. However, both methods are very empirical. These measurements will in future need to be collected in situ in order to develop valid parameterizations for snow drift.

The surface temperatures of snow, soil, and water are critical boundary conditions for solving finite difference equations; they are dependent on atmospheric conditions as well as the snow/soil/water conditions (Yi et al., 2013). In models with hourly time steps, snow/soil/water surface temperatures are calculated by iteratively solving the surface energy balance equation for the different surfaces.. This involves incoming and reflected solar radiation, incoming and outgoing longwave radiation, sensible and latent heat fluxes between the surface and the atmosphere, and ground heat flux (Oleson et al., 2004). In this study we have used a regression model to calculate surface temperatures on the basis of existing measurements. These algorithms performed better for the rim and center sites than for the pond and lake sites. The exchange of energy in water bodies is not only a result of molecular diffusion and eddy diffusion, but also of other processes such as convection caused by water density instability and complex lake-bottom shapes, which have not been taken into account in this study. We followed Subin et al. (2012) to simulate these effects implicitly by increasing the eddy diffusion coefficient. For example, in order to fit with the dynamics of water temperature at bottom of the lake (6 m) at the lake site, the eddy diffusion coefficient had to be increased by at least a factor of 10 (Fig. 9). Extensive work is required to test this approach over other lakes in different regions.

The lateral heat gradients under different land surfaces of the polygonal tundra landscape were obvious (Fig. 11). However, the DOS-TEM is a one-dimension model, which is therefore unable to simulate lateral heat exchange. A 2- or 3-dimensional model would be better able to simulate thermal processes in complex Arctic tundra landscapes (e.g., Ling and Zhang, 2003; Plug and West, 2009; van Huissteden et al., 2011; Kessler et al., 2012), but such models are difficult to apply overlarge regions.

Thermal processes vary under the different land surfaces of the heterogeneous polygonal tundra. For example, a talik was present under the lake site, but not under the center or pond sites. In our study we have assumed fixed shapes for polygon centers and for thermokarst lakes. It would, however, be desirable to include the dynamics of thermokarst lake development in future studies.

5 Conclusions

In this study we have modified an ecosystem model to simulate thermal processes under the different land surface types of a polygonal tundra landscape on Samoylov Island, in the Lena Delta of Siberia. The simulated freeze-thaw dynamics and soil/water temperatures compared very well with analytical Neumann solutions for three different materials in idealized runs. Despite a number of limitations and uncertainties relating to model parameterization and data input, the simulated soil/water temperatures compared reasonable well with in situ measurements. The modified model is also very efficient and is suitable for large scale regional applications.

Water has an important influence on the different thermal processes that operate under the various land surface types. Sensitivity tests indicate that thermal processes are very sensitive to changes in water depth when the depth is between approximately 1 and 2 m. The different land surface types of polygonal tundra ecosystems need to be taken into account in large scale ecosystem models in order to be able to accurately simulate methane emission. Modeling of thermal processes should at the very least take into account the following land surface types: polygon rims, polygon centers with maximum water depths of less than 1.2 m, and lakes with water depths of both less than 2 m and greater than 2 m.

Appendix A

Modelling the effects of water

The low-centered polygon landscape of the Arctic tundra can be simplified into polygon rims, polygon centers (with and without water) of various sizes, and lakes of various sizes. On the basis of the original soil and snow structure of the DOS-TEM (the previous version of the DOS-TEM had no water), we modeled water bodies above soil layers (Figure A1a) to simulate the effects that the water in polygon centers and lakes has on freezing or thawing dynamics in the underlying soils or sediments. The division of water into layers was the same as that for soils, i.e. 2 cm, 4 cm, 8 cm, …, 2^n cm, where n is the layer index.

A1 Effects of slope on volumetric water content

The slope between a polygon center and its rim (and also between a lake floor and its shoreline) was set to 28° in our model (Fig. A2), on the basis of field observations. The vertical distance between the bottom of a polygon center (or of a lake) and the top of its rim was taken to be the maximum water depth ($\mathrm{WD}_{\mathrm{max}}$). We assumed the shape of polygon center (or lake) to resemble part of an inverted cone, with a radius of r_{bot} at the bottom and r_{top} at the top.

The volumetric water content (vwc) of a water layer i can then be expressed as:

$$\mathrm{vwc}_i = \frac{V_{\mathrm{top},i} - V_{\mathrm{bot},i}}{V_{\mathrm{cyl}}} + \frac{V_{\mathrm{cyl}} - (V_{\mathrm{top},i} - V_{\mathrm{bot},i})}{V_{\mathrm{cyl}}}\theta \tag{A1}$$

where

$$V_{\mathrm{top},i} = \frac{1}{3}\pi r_{\mathrm{top},i}^2 (\mathrm{d}x_i + h) \tag{A2}$$

$$V_{\mathrm{bot},i} = \frac{1}{3}\pi r_{\mathrm{bot},i}^2 h \tag{A3}$$

$$V_{\mathrm{cyl}} = \pi r_{\mathrm{top}}^2 \mathrm{d}x_i \tag{A4}$$

GMDD
6, 4883–4932, 2013

$$h = \frac{r_{\mathrm{bot},i}}{\tan(\pi\frac{28}{180})} \tag{A5}$$

$$r_{\mathrm{bot}} = r_{\mathrm{top}} - \mathrm{WD}_{\max}\tan(\pi\frac{28}{180}) \tag{A6}$$

In these equations $r_{\mathrm{top},\,i}$ and$r_{\mathrm{bot},\,i}$ are the top and bottom radii of layer i, $\mathrm{d}x_i$ is the thickness of layer i, h is the vertical distance from the top of the cone to the plane with a radius of $r_{\mathrm{bot},\,i}$, θ (= 0.6 in this study) is the volumetric water content of the soil rim around the water layers. Field survey results on the Samoylov Island indicate that $\mathrm{WD}_{\max} = 173.1\ln(r_{\mathrm{top}}) - 231.45$ ($R^2 = 0.99$, $n = 12$; Wischnewski, 2013). In Table A1 we present examples for a small polygon, a large polygon, and a lake.

A2 Thermal dynamics in water

The exchange of energy within water is affected by several processes including molecular diffusion, wind-driven eddy diffusion, buoyant convection, amongst others. In the DOS-TEM we took into account molecular diffusion, eddy diffusion (which is usually 2–3 orders greater than molecular diffusion, Subin et al., 2012), and other processes by increasing the eddy diffusion coefficient by a factor of between 10 and 100. In cold seasons with snow and ice cover, the dissipation of energy to the atmosphere would only be realized by molecular diffusion, while in warm seasons with open water the exchange of energy within the water would be much greater. The seasonal variation in energy exchange coefficients is therefore an important factor in the development of unfrozen soil beneath water bodies. Water layers were treated in the same way as soil and snow layers but with different thermal properties (Fig. A1a) when calculating the positions of freezing or thawing fronts and the temperatures in water bodies. Following Hostetler and Bartlein (1990), the governing equation for the one-dimensional model is:

$$C\frac{\partial T}{\partial t} = \frac{\partial}{\partial z}\left((\lambda + CK)\frac{\partial T}{\partial z}\right) + \frac{\partial \Phi}{\partial z} \tag{A7}$$

where T is the water/soil/snow temperature (K), t is the time (s), z is the depth from water surface (m), C is the volumetric heat capacity (J (m^{-3} K)), λ is the thermal conductivity of water/soil/snow (J mKs^{-1}), K is the conductivity due to eddy diffusion (for water only, J (mKs)$^{-1}$), and Φ is a heat source term (w m^{-2}). The detailed parameterization of K and Φ can be found in Hostetler and Bartlein (1990).

Appendix B

Soil thermal conductivity

In this study, we applied a soil thermal conductivity scheme proposed by Luo et al. (2009), which integrated the schemes of Johansen (1975) and Côté and Konrad (2005), as follows:

$$k = \begin{cases} K_e k_{\text{sat}} + (1 - K_e) k_{\text{dry}} \; S_r > 1 \times 10^{-5} \\ k_{\text{dry}} \; S_r \leq 1 \times 10^{-5} \end{cases} \tag{B1}$$

$$k_{\text{sat}} = \begin{cases} k_s^{1-\theta_{\text{sat}}} k_{\text{liq}}^{\theta_{\text{sat}}} \; T \geq T_f \\ k_s^{1-\theta_{\text{sat}}} k_{\text{liq}}^{\theta_{\text{sat}}} k_{\text{ice}}^{\theta_{\text{sat}}-\theta_{\text{liq}}} \; T < T_f \end{cases} \tag{B2}$$

$$k_s = k_q^{q} k_o^{1-q} \tag{B3}$$

GMDD
6, 4883–4932, 2013

Title Page
Abstract Introduction
Conclusions References
Tables Figures
◀◀ ▶▶
◀ ▶
Back Close
Full Screen / Esc
Printer-friendly Version
Interactive Discussion

$$k_{dry} = \chi \times 10^{-\eta\theta_{sat}} \quad \text{(B4)}$$

$$K_e = \frac{\kappa S_r}{1 + (\kappa - 1)S_r} \quad \text{(B5)}$$

where k, k_{sat}, k_{dry}, k_s, k_{liq}, k_{ice}, k_q, and k_o are thermal conductivities (W/(mK)) of soil, saturated soil, dry soil, soil solid, unfrozen(liquid) water, ice, quartz sand, and other components, respectively. θ_{sat} and θ_{liq} are the porosity and the liquid water content of soil (%), respectively. K_e is the Kersten number. S_r is the soil saturation. χ, η, and κ are 3 parameters whose values for different soil types can be found in Côté and Konrad (2005).

Acknowledgements. This study was supported through grants provided as part of the National Basic Research Program (973 Programme) (2013CBA01807 and 2010CB951402), the Strategic Priority Research Program (XDB030303) and One Hundred People Plan (O927581001) of the Chinese Academy of Sciences. We are grateful to the German Academic Exchange Service (DAAD) for providing support for the first author to visit Germany. This work was also supported by the European Union FP7-ENV PAGE21 project (contract No. 9 GA282700).

References

Abnizova, A., Siemens, J., Langer, M., and Boike, J.: Small ponds with major impact: The relevance of ponds and lakes in permafrost landscapes to carbon dioxide emissions, Global Biogeochem. Cy., 26, GB2041, doi:10.1029/2011GB004237, 2012.

Arain, M. A., Burke, E. J., Yang, Z.-L., and Shuttleworth, W. J.: Implementing surface parameter aggregation rules in the CCM3 global climate model: regional responses at the land surface, Hydrol. Earth Syst. Sci., 3, 463–476, doi:10.5194/hess-3-463-1999, 1999.

Boike, J., Kattenstroth, B., Abramova, K., Bornemann, N., Chetverova, A., Fedorova, I., Fröb, K., Grigoriev, M., Grüber, M., Kutzbach, L., Langer, M., Minke, M., Muster, S., Piel, K., Pfeiffer, E.-M., Stoof, G., Westermann, S., Wischnewski, K., Wille, C., and Hubberten, H.-W.: Baseline characteristics of climate, permafrost and land cover from a new permafrost observatory in the Lena River Delta, Siberia (1998–2011), Biogeosciences, 10, 2105–2128, doi:10.5194/bg-10-2105-2013, 2013.

Brown, J., Ferrians Jr., O. J., Heginbottom, J., and Melnikov, E.: Circum-Arctic map of permafrost and ground-ice conditions, National Snow and Ice Data Center/World Data Center for Glaciology, Boulder, CO, 1998.

Clein, J. S., McGuire, A. D., Euskirchen, E. S., and Calef, M. P.: The effects of different climate input datasets on simulated carbon dynamics in the Western Arctic, Earth Interactions, 11, doi:10.1175/EI229.1, 2007.

Côté, J. and J. Konrad: A generalized thermal conductivity model for soils and construction materials, Can. Geotech. J. 42, 443–458, 2005.

Cresto Aleina, F., Brovkin, V., Muster, S., Boike, J., Kutzbach, L., Sachs, T., and Zuyev, S.: A stochastic model for the polygonal tundra based on Poisson-Voronoi diagrams, Earth Syst. Dynam., 4, 187–198, doi:10.5194/esd-4-187-2013, 2013.

Dall'Amico, M., Endrizzi, S., Gruber, S., and Rigon, R.: A robust and energy-conserving model of freezing variably-saturated soil, The Cryosphere, 5, 469–484, doi:10.5194/tc-5-469-2011, 2011.

Etzelmüller, B. and Frauenfeld, R.: Factors controlling the distribution of mountain permafrost in the northern hemisphere and their influence on sediment transfer, Arct. Alp. Res., 41, 48–58, 2009.

Farouki, O. T.: Thermal properties of soils, Cold Reg. Res. and Eng. Lab., Hanover, N. H, 1986.

Fox, J. D.: Incorporating Freeze-Thaw Calculations into a water balance model, Water Resour. Res., 28, 2229–2244, 1992.

French, H.: ThePeriglacial Environment, 3rd, John Wiley & Sons, Ltd, 2007.

Goodrich, E. L.: Efficient Numerical Technique for one-dimensional Thermal Problems with phase change, Int. J. Heat Mass Transfer, 21, 615–621, 1978.

Hipp, T., Etzelmüller, B., Farbrot, H., Schuler, T. V., and Westermann, S.: Modelling borehole temperatures in Southern Norway – insights into permafrost dynamics during the 20th and 21st century, The Cryosphere, 6, 553–571, doi:10.5194/tc-6-553-2012, 2012..

Hostetler, S. W. and Bartlein, P. J.: Simulation of Lake Evaporation with Application to Modeling Lake Level Variations of Harney-Malheur Lake, Oregon, Water Resour. Res., 26, 2603–2612, 1990.

Johansen, O.: Thermal conductivity of soils, Ph. D. thesis, University of Trondheim, 1975.

Jumikis, A. R.: Thermal Geotechnics, Rutgers Univ. Press, New Brunswick, N. J., 1375 pp., 977.
Kessler, M. A., Plug, L. J., and Walter, K. M.: Simulating the decadal- to millennial-scale dynamics of morphology and sequestered carbon mobilizaion of two thermokarst lakes in NW Alaska, J. Geophys. Res., 117, G00M06, doi:10.1029/2011JG001796, 2012.
Langer, M., Westermann, S., Muster, S., Piel, K., and Boike, J.: The surface energy balance of a polygonal tundra site in northern Siberia – Part 2: Winter, The Cryosphere, 5, 509–524, doi:10.5194/tc-5-509-2011, 2011.
Langer, M., Westermann, S., Heikenfeld, M., Dorn, W., and Boike, J.: Satellite-based modeling of permafrost temperatures in a tundra lowland landscape, Remote Sens. Environ., 135, 12–24, 2013.
Lawrence, D. M. and Slater, A. G.: Incorporating organic soil into a global climate model, Clim. Dyn., 30, 145–160, 2008.
Ling, F. and Zhang, T.: Numerical simulation of permafrost thermal regime and talik development under shallow thaw lakes on the Alaskan Arctic Coastal Plain, J. Geophys. Res., 108, 4511, doi:10.1029/2002JD003014, 2003.
Lunardini V. J.: Heat transfer in cold climates, Van Nostrand Reinhold: New York, 1981.
Luo, S., Lv, S., Zhang, Y., Hu, Z., Ma, Y., Li, S., and Shang, L.: Soil thermal conductivity parameterization establishment and application in numerical model of central Tibetan Plateau, Chinese J. Geophys., 52, 919–928, 2009 (in Chinese with English Abstract).
Manabe, S.: Climate and the ocean circulation: I. the atmospheric circulation and the hydrology of the Earth's surface, Mon. Weather Rev., 97, 739–774, 1969.
McGuire, A. D., Melillo, J., Jobbagy, E. G., Kicklighter, D., Grace, A. L., Moore, B., and Vorosmarty, C. J.: Interactions Between Carbon and Nitrogen Dynamics in Estimating Net Primary Productivity for Potential Vegetation in North America, Global Biogeochem. Cy., 6, 101–124, 1992.
McGuire, A. D., Anderson, L. G., Christensen, T. R., Dallimore, S., Guo, L., Hayes, D. J., Heimann, M., Lorenson, T. D., MacDonald, R. W., and Roulet, N. T.: Sensitivity of the carbon cycle in the Arctic to climate change, Ecol. Monogr., 79, 523–555, 2009.
Muster, S., Langer, M., Heim, B., Westermann, S., and Boike, J.: Subpixel heterogeneity of ice-wedge polygonal tundra: a multi-scale analysis of land cover and evapotranspiration in the Lena River Delta, Siberia, Tellus B, 64, 17301, doi:10.3402/tellusb.v64i0.17301, 2012.

Muster, S., Heim, B., Abnizova, A., and Boike, J.: Water body distributions across scales: A remote sensing based comparison of three arctic tundra wetlands. Remote Sens., 5, 1498–1523, 2013.
NASA Landsat Program: Lena Delta in Landsat 7/ETM+, Visible Earth, v1 ID: 407 18024, available at: http://visibleearth.nasa.gov/ (access: 10 October 2011), 2000.
Nicolsky, D. J., Romanovsky, V. E., Alexeev, V. A., and Lawrence, D. M.: Improved modeling of permafrost dynamics in a GCM land-surface scheme, Geophys. Res. Lett., 34, L08501, doi:10.1029/2007GL029525, 2007.
Oleson, K. W., Dai, Y., Bonan, G. B., Bosilovich, M. G., Dickinson, R. E., Dirmeyer, P., Hoffman, F., Houser, P. R., Levis, S., Niu, G.-Y., Thornton, P., Vertenstein, M., Yang, Z.-L., and Zeng, X.: Technical description of the Community Land Model(CLM), Tech. Rep., NCAR/TN-461+STR, Natl. Cent. for Atmos. Res., Boulder, Colo., 2004.
Parsekian, A. D., Grosse, G., Walbrecker, J. O., Muller-Petke, M., Keating, K., Liu, L., Jones, B. M., and Knight, R.: Detecting unfrozen sediments below thermokarst lakes with surface nuclear magnetic resonance, Geophys. Res. Lett., 40, 535–540, 2013.
Plug, L. J. and West, J. J.: Thaw lake expansion in a two-dimensional coupled model of heat transfer, thaw subsidence, and mass movement, J. Geophys. Res., 114, F01002, doi:10.1029/2006JF000740, 2009.
Pollack, H., Hurter, S., and Johnson, J.: Heat flow from the Earth's interior: Analysis of the global data set, Rev. Geophys., 31, 267–280, 1993.
Ringeval, B., Decharme, B., Piao, S., Ciais, P., Papa, P., Noblet-Ducoudré, N., Prigent, C., Friedlingstein, P., Gouttevin, I., and Koven, C.: Modelling sub-grid wetland in the ORCHIDEE global land surface model: evaluation against river discharges and remotely sensed data, Geosci. Model Dev., 5, 941–962, 2012.
Riseborough, D. W., Shiklomanov, N. I., Etzelmüller, B., Gruber, S., and Marchenko, S.: Recent Advances in Permafrost Modelling, Permafrost Periglac., 19, 137–156, 2008.
Romanovsky, V. E. and Osterkamp, T. E.: Thawing of the Active Layer on the Coastal Plain of the Alaskan Arctic, Permafrost Periglac., 8, 1–22, 1997.
Schneider von Deimling, T., Meinshausen, M., Levermann, A., Huber, V., Frieler, K., Lawrence, D. M., and Brovkin, V.: Estimating the near-surface permafrost-carbon feedback on global warming, Biogeosciences, 9, 649–665, doi:10.5194/bg-9-649-2012, 2012.

GMDD
6, 4883–4932, 2013

Modeling different freeze/thaw processes in landscapes

S. Yi et al.

Sturm, M., McFadden, J. P., Liston, G. E., Chapin, S. F., Racine, C., and Holmgren, J.: Snow-Shrub Interactions in Arctic Tundra: A Hypothesis with Climatic Implications, J. Climate, 14, 336–344, 2001.
Subin, Z. M., Riley, W. J., and Mironov, D.: An improved lake model for climate simulations: Model structure, evalution, and sensitivity analyses in CESM1, J. Adv. Model. Earth Sys., 4, M02001, doi:10.1029/2011MS000072, 2012.
van Huissteden, J., Berrittella, C., Parmentier, F. J., Mi, Y., Maximov, T. C., and Dolman, A. J.: Methane emissions from permafrost thaw lakes limited by lake drainage, Nature Climate Change, 1, 119–123, 2011.
Wania, R., Ross, I., and Prentice, C. I.: Integrating peatlands and permafrost into a dynamic global vegetation model: 1. Evaluation and sensitivity of physical land surface processes, Global Biogeochem. Cy., 23, GB3014, doi:10.1029/2008GB003412, 2009.
Wischnewski, K.: Temperature Simulation Model for Small Water Bodies in the Arctic Tundra, Lena River Delta (Siberia, Russia), Master thesis, Swiss Federal Institute of Technology Zurich, http://epic.awi.de/32775/, 2013.
Woo, M.-K., Arain, A. M., Mollinga, M., and Yi, S.: A two-directional freeze and thaw algorithm for hydrologic and land surface modelling, Geophys. Res. Lett., 31, L12501, doi:10.1029/2004GL019475, 2004.
Yi, S., Arain, A. M., and Woo, M.-K.: Modifications of a land surface scheme for improved simulation of ground freeze-thaw in northern environments, Geophys. Res. Lett., 33, L13501, doi:10.1029/2006GL026340, 2006.
Yi, S., Woo, M.-K., and Arain, A. M.: Impacts of peat and vegetation on permafrost degradation under climate warming, Geophys. Res. Lett., 34, L16504, doi:10.1029/2007/GL030550, 2007.
Yi, S., McGuire, A. D., Harden, J., Kasischke, E., Manies, K. L., Hinzman, L. D., Liljedahl, A., Randerson, J. T., Liu, H., Romanovsky, V. E., Marchenko, S., and Kim, Y.: Interactions between soil thermal and hydrological dynamics in the response of Alaska ecosystems to fire disturbance , J. Geophys. Res., 114, G02015, doi:10.1029/2008JG000841, 2009a.
Yi, S., Manies, K. L., Harden, J., and McGuire, A. D.: The characteristics of organic soil in black spruce forests: Implications for the application of land surface and ecosystem models in cold regions, Geophys. Res. Lett., 36, L05501, doi:10.1029/2008GL037014, 2009b.
Yi, S., McGuire, A. D., Kasischke, E., Harden, J., Manies, K. L., Mack, M., and Turetsky, M. R.: A Dynamic organic soil biogeochemical model for simulating the effects of wildfire on soil

GMDD
6, 4883–4932, 2013

Modeling different freeze/thaw processes in landscapes

S. Yi et al.

environmental conditions and carbon dynamics of black spruce forests, J. Geophys. Res., 115, G04015, doi:10.1029/2010JG001302, 2010.
Yi. S., Li, N., Xiang, B., Ye, B., and McGuire, A. D.: Representing the effects of alpine grassland vegetation cover on the simulation of soil thermal dynamics by ecosystem models applied to the Qinghai-Tibetan Plateau, J. Geophys. Res., 118, 1–14, doi:10.1002/jgrg.20093, 2013.
Zhang, Y., Chen, W., and Cihlar, J.: A process-based model for quantifying the impact of climate change on permafrost thermal regimes, J. Geophys. Res.-Atmos., 108, 4695, doi:10.1029/2002JD003354, 2003.
Zhang, Y., Chen, W., and Riseborough, D. W.: Disequilibrium response of permafrost thaw to climate warming in Canada over 1850–2100, Geophys. Res. Lett., 35, L02502, doi:10.1029/2007GL032117, 2008.
Zhang, Y., Sachs, T., Li, C., and Boike, J.: Upscaling methane fluxes from closed chambers to eddy covariance based on a permafrost biogeochemistry integrated model, Global Change Biol., 18, 1428–1440, 2012.
Zhuang, Q., Romanovsky, V. E., and McGuire, A. D.: Incorporation of a permafrost model into a large-scale ecosystem model: Evaluation of temporal and spatial scaling issues in simulating soil thermal dynamics, J. Geophys. Res., 106, 33649–33670, 2001.
Zhuang, Q., Melillo, J., Sarofim, M. C., Kicklighter, D., McGuire, A. D., Felzer, B. S., Sokolov, A., Prinn, R. G., Steudler, P. A., and Hu, S.: CO_2 and CH4 exchanges between land ecosystems and the atmosphere in northern high latitudes over the 21st century, Geophys. Res. Lett., 33, L17403, doi:10.1029/2006GL026972, 2006.

GMDD
6, 4883–4932, 2013

Table 1. The thermal conductivity, volumetric heat capacity, volumetric water content, and porosity used in idealized runs for water, mineral soils, and organic soils.

	Thermal Conductivity ($\mathrm{J\,mKs^{-1}}$)		Volumetric Heat Capacity ($10^6\ \mathrm{J\,m^{-3}}$)		Volumetric Water Content (%)	Porosity (%)
	Frozen	Unfrozen	Frozen	Unfrozen		
Water	2.29	0.6	2.12	4.19	100	100
Mineral	2.69	1.71	2.06	2.79	33.28	39
Organic	0.37	0.21	0.99	1.84	36.25	90

GMDD
6, 4883–4932, 2013

Modeling different freeze/thaw processes in landscapes

S. Yi et al.

Table 2. Water and organic soil configurations used in the model for the different test sites.

	Maximum water depth (m)	Water depth (m)	Organic soil
rim	N.A.	N.A.	3 cm moss (dry organic, porosity $p = 0.95$, volumetric water content vwc = 0.3) 20 cm organic rich soil (wet organic, $p = 0.9$, vwc = 0.7)
center	0.25	0	1 m organic soil (saturated organic, $p = 0.9$, vwc = 0.9)
pond	1.1	1.05	As for center
lake	6	6	As for center

GMDD
6, 4883–4932, 2013

Modeling different freeze/thaw processes in landscapes

S. Yi et al.

Table 3. Thermal properties of different types of soil on Samoylov Island. The first is derived using soil temperature measurements; the second is calculated using the default scheme in the DOS-TEM.

	Thermal Conductivity ($W\,mK^{-1}$)		Volumetric Heat Capacity ($MJ\,m^{-3}K$)		Thermal diffusivity) ($10^{-6}\,m^2\,s^{-1}$)	
	Unfrozen	Frozen	Unfrozen	Frozen	Unfrozen	Frozen
Dry organic	0.14/0.17	0.46/0.29	0.9/1.43	0.7/0.75	0.30/0.59	0.66/0.39
Wet organic	0.6/0.30	0.95/0.57	3.4/2.6	1.8/1.44	0.18/0.12	0.53/0.40
Saturated organic	0.72/0.54	1.92/1.83	3.8/4.02	2.0/2.16	0.19/0.13	0.96/0.95
Mineral	N.A./1.00	1.9/2.12	N.A./3.16	2.0/2.04	N.A./0.32	0.95/1.03

GMDD
6, 4883–4932, 2013

Table 4. The root mean squared error ($n = 36\,500$) between the thawing fronts (m) from exact Neumann solutions and simulated thawing fronts from the DOS-TEM, with different combinations of total thickness (50, 500, and 5000 m) and bottom-up forcing (b1m: bottom-up forcing at 1 m below front; nobot: no bottom-up forcing) for different materials.

	5000 m, b1m	5000 m, nobot	500 m, b1m	50 m, b1m
Water	0.004	1.253	0.032	0.274
Mineral	0.062	4.645	0.177	1.899
Organic	0.012	1.128	0.047	0.065

GMDD
6, 4883–4932, 2013

Table 5. The root mean squared error ($n = 36\,500$) between the temperatures (°C) from exact Neumann solutions and simulated temperatures from the DOS-TEM for different materials, with 5000m total thickness and bottom-up forcing at 1 m below the thawing front, at depths between 0.05 and 20 m.

	0.05	0.1	0.5	1	3	6	9	15	20
Water	0.018	0.017	0.044	0.054	0.039	0.039	0.041	0.087	0.071
Mineral	0.011	0.018	0.014	0.010	0.016	0.027	0.030	0.057	0.062
Organic	0.019	0.016	0.009	0.009	0.024	0.042	0.047	0.111	0.110

GMDD
6, 4883–4932, 2013

Table A1. The area, top radius (r_{top}), bottom radius (r_{bot}), maximum water depth (WD_{max}) of polygons or lakes, and their volumetric water contents (vwc) at the top and bottom.

	Area (m^2)	r_{top} (m)	r_{bot} (m)	WD_{max} (m)	VWC	
					Top layer	Bottom layer
Small polygon	50[a]	3.99	3.95	0.08	1	0.99
Large polygon	200[b]	7.98	7.30	1.28	1	0.94
Lake	39541[c]	112.19	109.07	5.86	1	0.98

[a] Mean average surface area of the smallest polygon centers on Samoylov Island (Wischnewski, 2013); [b] mean average surface area of the largest polygon centers surveyed on Samoylov Island; [c] area of the large thermokarst lake on Samoylov Island.

GMDD
6, 4883–4932, 2013

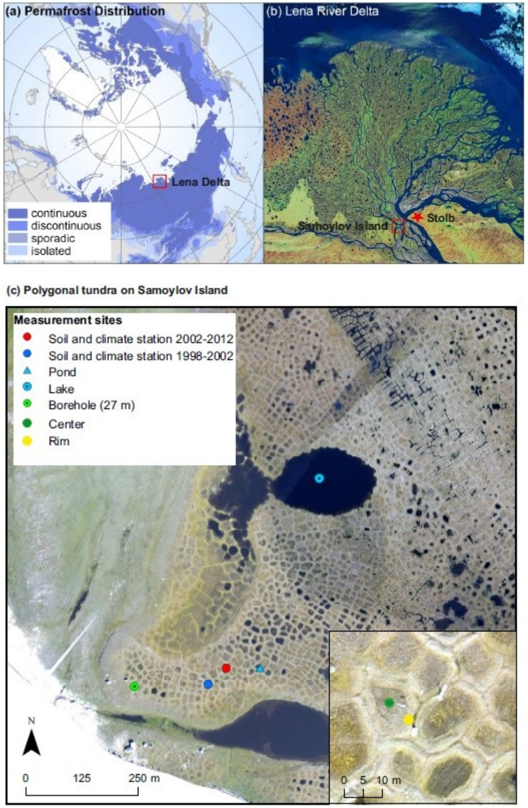

Fig. 1. (a) Circumpolar permafrost distribution (Brown et al., 1998) and the Lena River Delta; **(b)** Location of the Samoylov study site within the Lena River Delta, Eastern Siberia (NASA, 2000); and **(c)** locations of the measurements on the Samoylov Island.

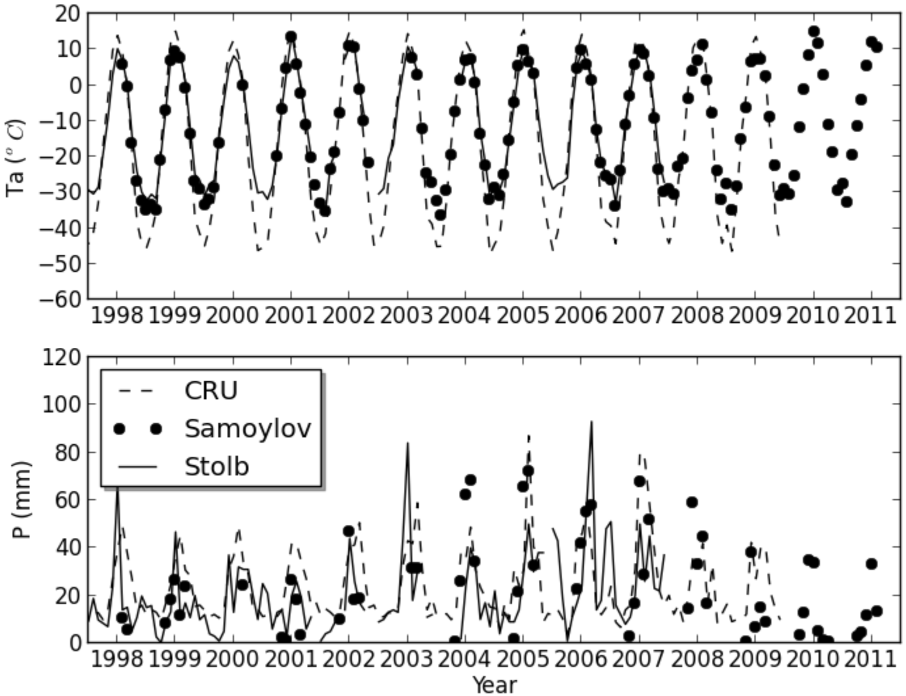

Fig. 2. Monthly air temperature (T_a) and precipitation (P) measurements from Samoylov Island (Samoylov), Stolb meteorological station (Stolb), and from the Climate Research Unit global dataset (CRU).

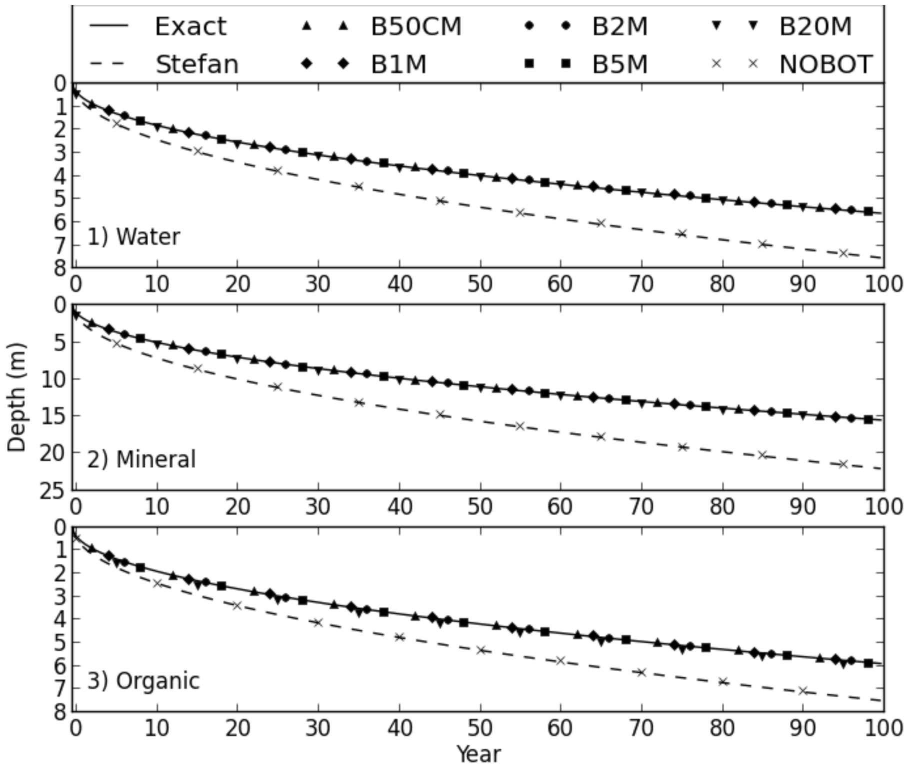

Fig. 3. Comparisons of outputs from DOS-TEM simulations, exact Neumann solutions (Exact), and Stefan's equation (Stefan) for (1) water, (2) mineral soil, and (3) organic soil over a one hundred year period. The term B50CM means simulations from the DOS-TEM with bottom-up forcing at 50 cm beneath the lowest freezing or thawing front, and likewise for other similar terms. NOBOT means no bottom-up forcing. The outputs from the DOS-TEM have been plotted for the middle of every tenth years and different cases have been started from different years in order to make the figures more readable.

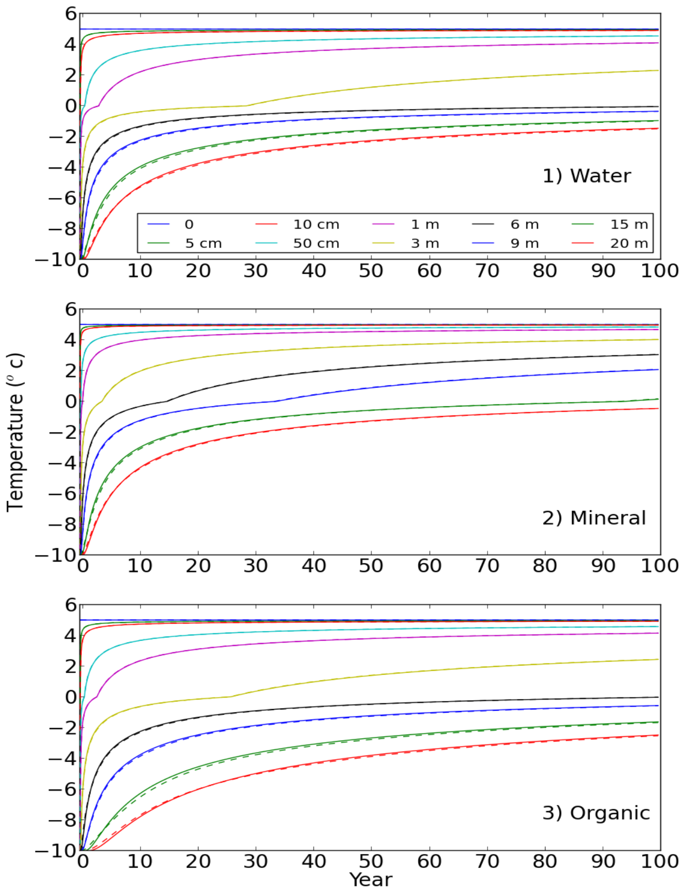

Fig. 4. Comparisons of outputs from DOS-TEM simulations (dashed lines) and exact Neumann solutions (solid lines) for (1) water, (2) mineral soil, and (3) organic soil over a period of one hundred years, at depths from 0 cm to 20 m.

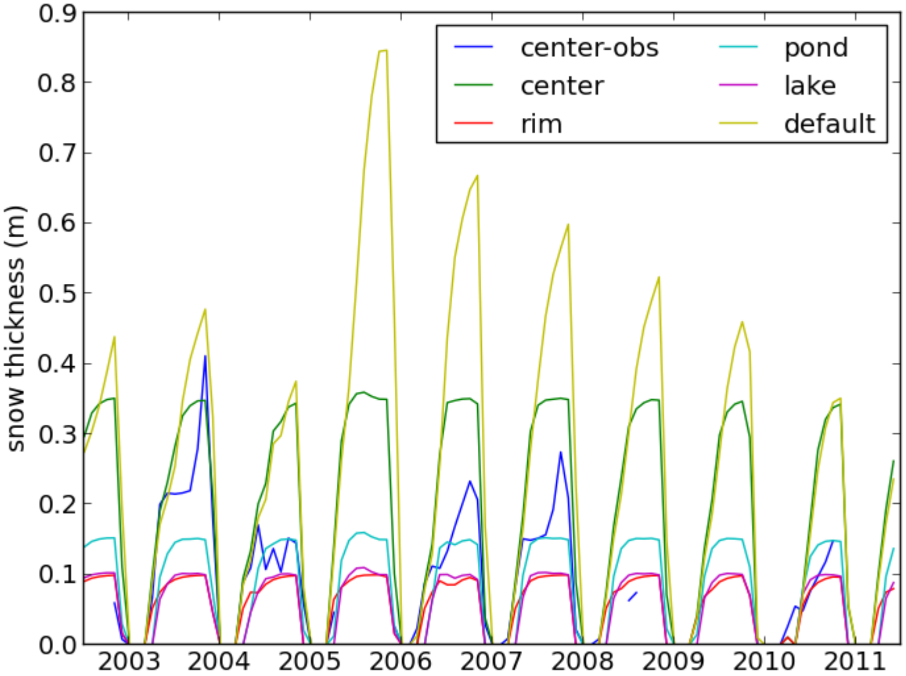

Fig. 5. Comparisons of simulated maximum (monthly) snow thicknesses at the center, rim, pond, and lake sites, the default values (with no maximum snow thickness set), with those from field measurements at the center site (center-obs), over the period from 2003–2011.

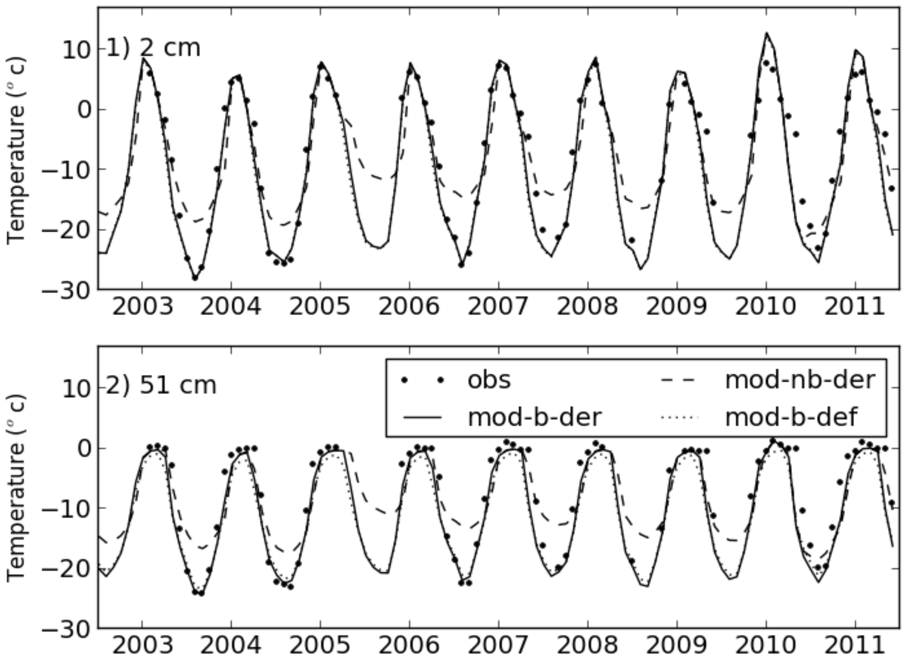

Fig. 6. Comparisons of monthly average soil temperatures at 2 cm and 51 cm depth below the rim site from simulations (mod), with and without a maximum snow thickness (*b* and *nb*), using derived and default thermal properties (der and def), with those from field measurements (obs), over the period from 2003–2011

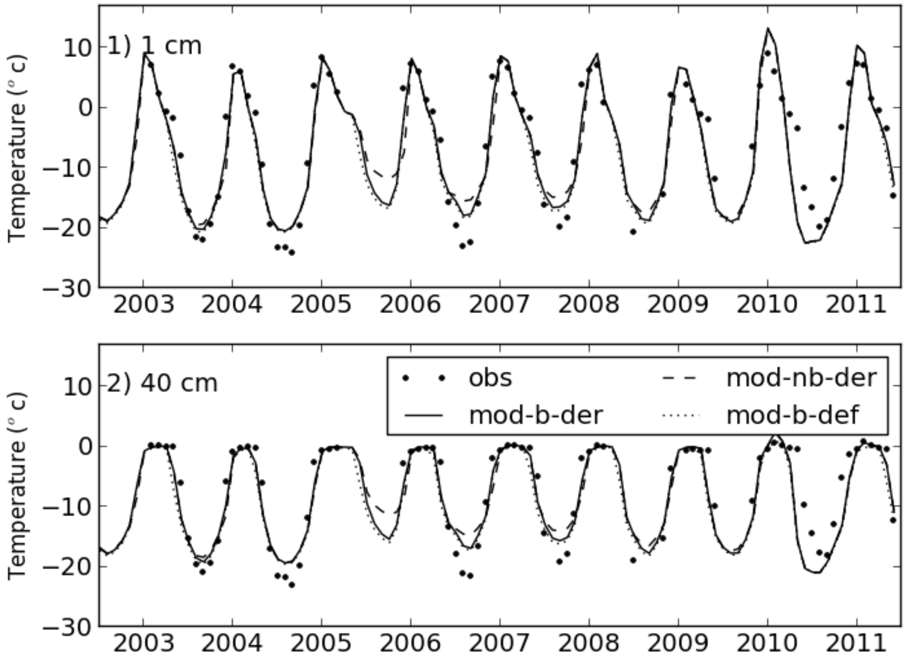

Fig. 7. Comparisons of monthly average soil temperatures at 1 and 40 cm depth below the *center* site from simulations (mod) with and without a maximum snow thickness setting (*b* and *nb*), using derived and default thermal properties (der and def), with those from field measurements (obs), over the period from 2003–2011.

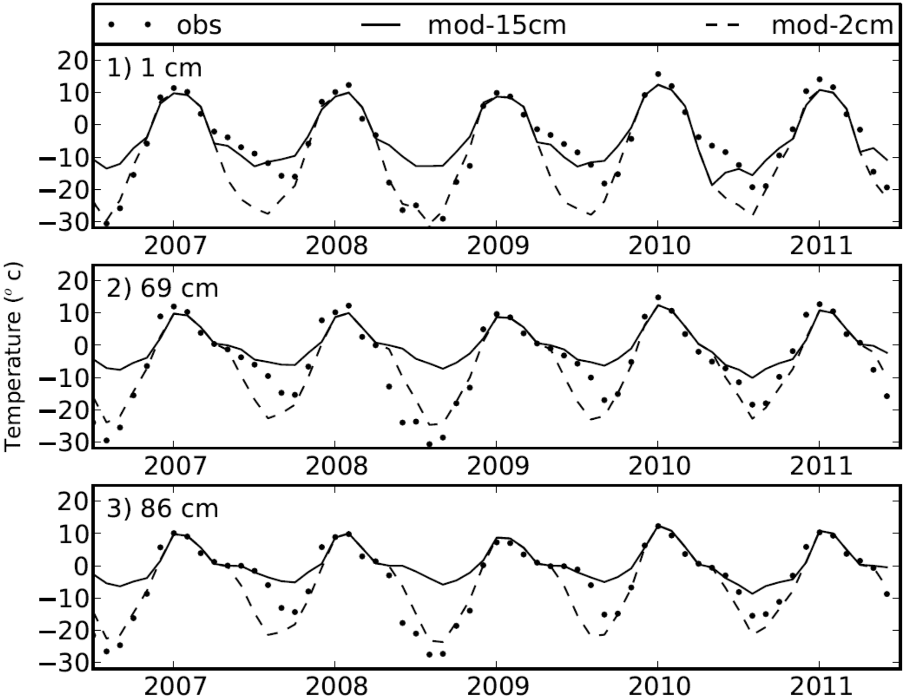

Fig. 8. Comparisons of monthly average water temperatures at 1, 69 and 86 cm depth below the water surface at the *pond* site from simulations with 15 cm (mod-15cm) and 2 cm (mod-2cm) maximum snow thickness, over the period from 2007–2011.

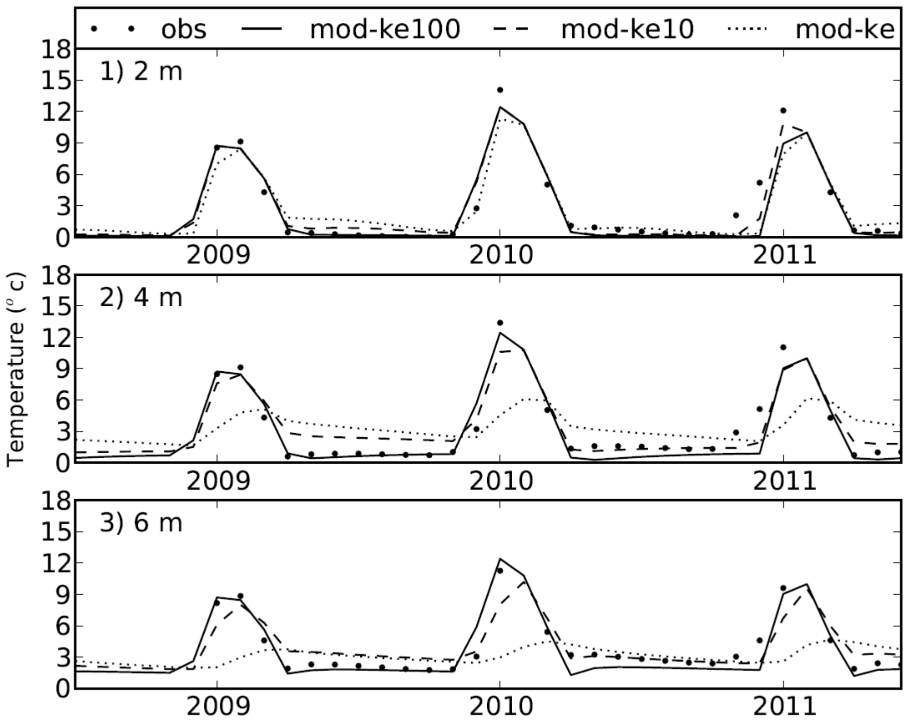

Fig. 9. Comparisons of monthly average water temperatures at 2, 4 and 6 m below the water surface at the *lake* site from simulations (mod) using default, 10 times, and 100 times the eddy diffusion coefficient (ke, ke10, and ke100) with field measurements (obs) over the period from 2009–2011.

GMDD
6, 4883–4932, 2013

Modeling different freeze/thaw processes in landscapes

S. Yi et al.

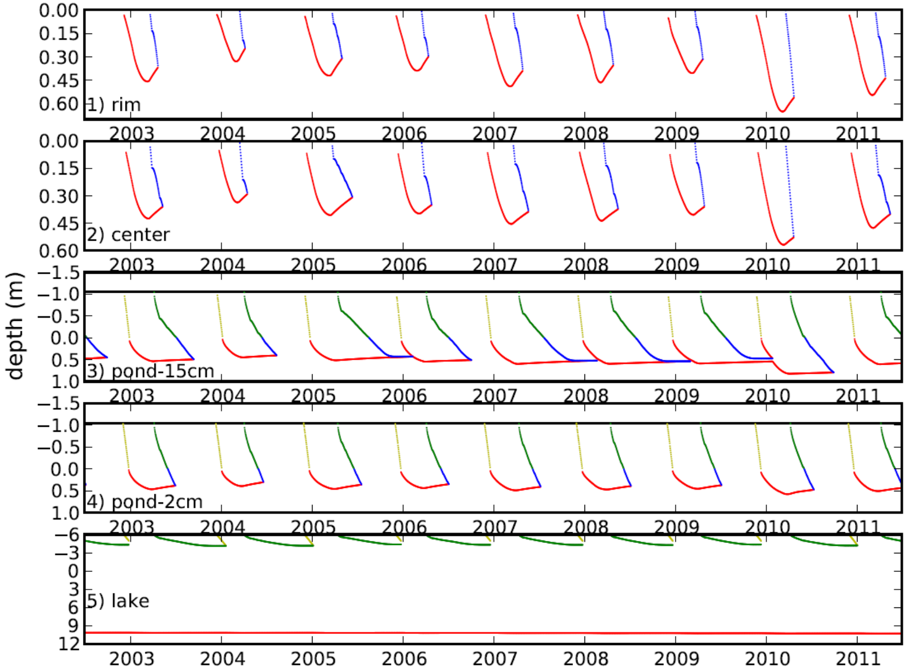

Fig. 10. Simulated soil freezing (blue) and thawing (red) fronts, and water freezing (green) and thawing (yellow) fronts (depths in meters) over the period from 2003–2011 for (1) the rim site, (2) the center site, (3) the pond site with 15 cm maximum snow thicknes *s*, (4) the pond site with 2 cm maximum snow thickness, and (5) the lake site. The surface of the soil was taken to be at 0 m depth, with the downward direction positive and the upward direction negative.

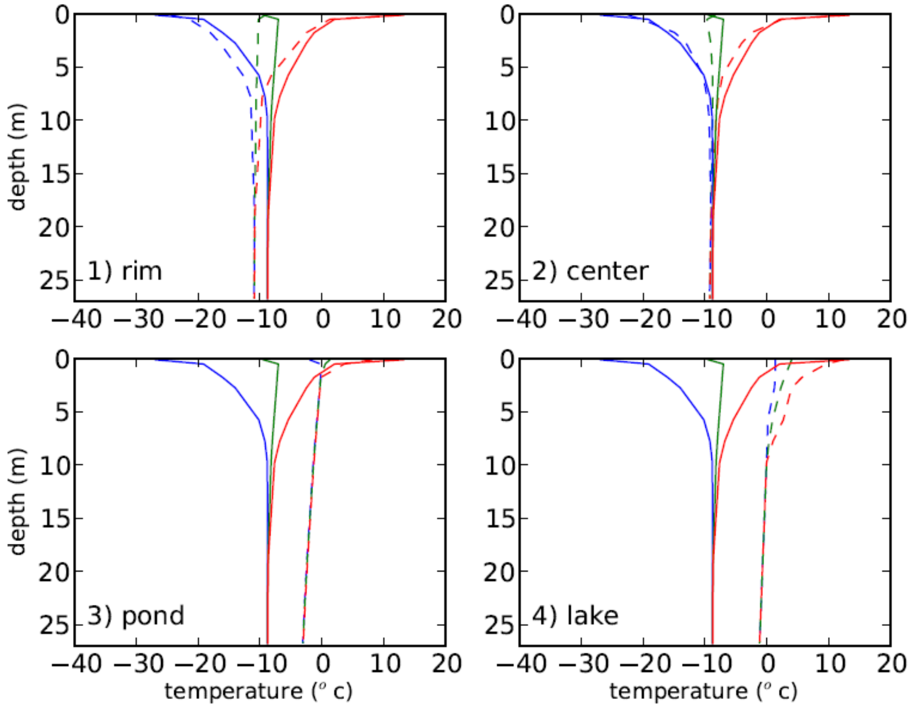

Fig. 11. Comparisons between simulated (dashed lines) and measured (solid lines) values for annual mean (green), maximum (red), and minimum (blue) soil temperatures (°C) averaged over the period from 2007–2011 for the (1) rim, (2) center, (3) pond, and (4) lake sites.

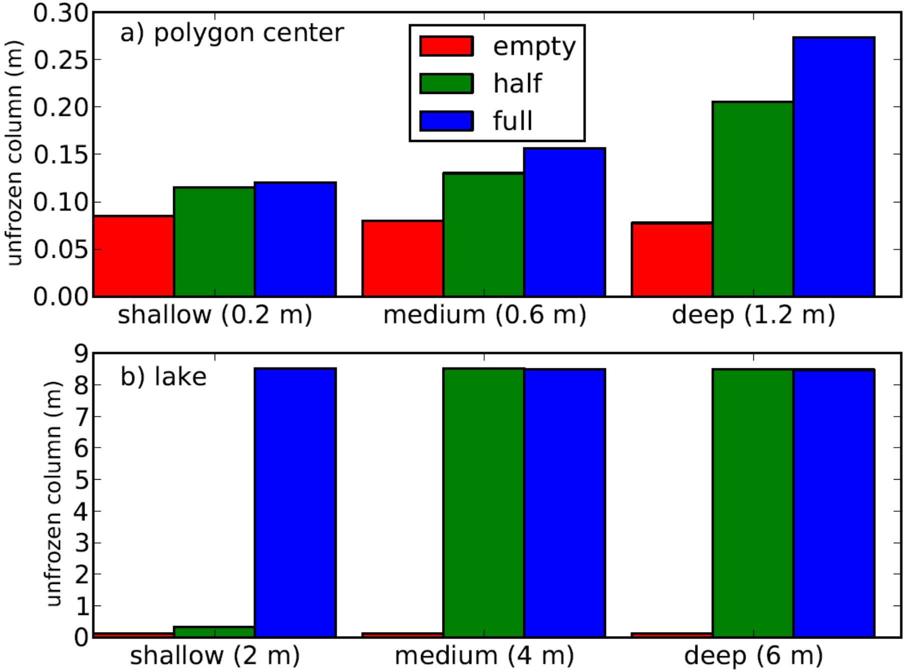

Fig. 12. Effect that water depth in polygon centers/lakes has on the mean unfrozen soil thickness over the period from 1981–2011. For polygon centers depths in **(a)**, shallow = 20 cm, medium = 60 cm, and deep = 120 cm. For lake depths in **(b)**, shallow = 2 m, medium = 4 m, and deep = 6 m. Empty, half full, and full refer to water depths that are 0, 50, and 100 of the maximum polygon center/lake depth, respectively.

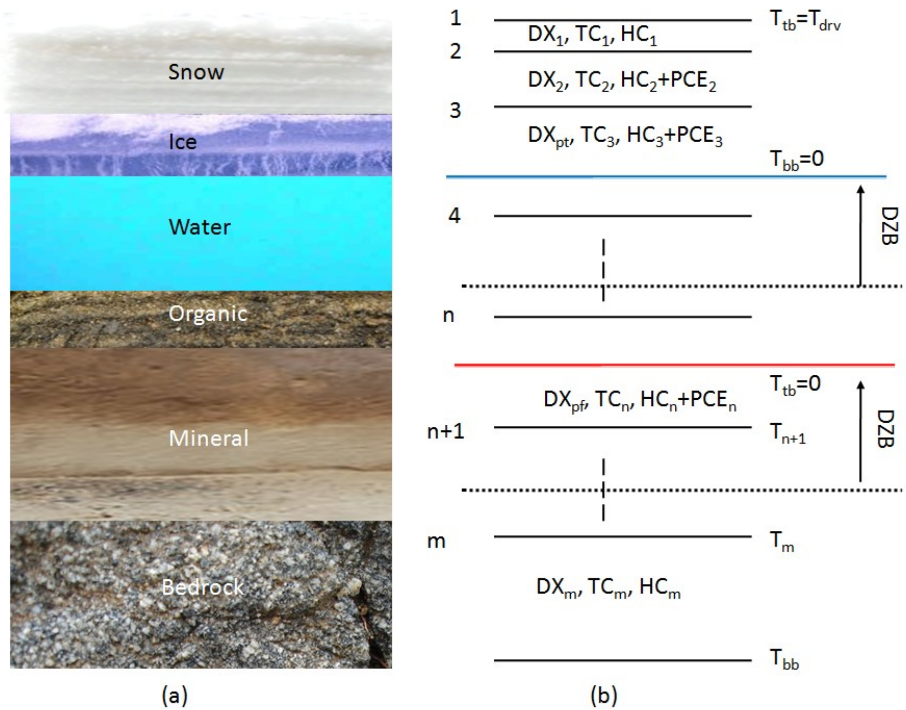

Fig. A1. The ground components considered in the DOS-TEM **(a)**, and a diagram of updating freezing and thawing fronts of ground components, together with temperatures **(b)**. DX, TC, HC, and PCE stand for thickness, thermal conductivity, heat capacity, and energy used for phase change, respectively; m and n are layer indexes; DZB is the distance between the bottom-up driving depth and the depth of the front. T_{tb}, T_{bb}, and T_{drv} are the top boundary, bottom boundary and ground surface driving temperature, respectively. The T_{bb} at the bottom of the ground structure is determined by the temperature and thermal properties of the overlying layer and the prescribed heat flux.

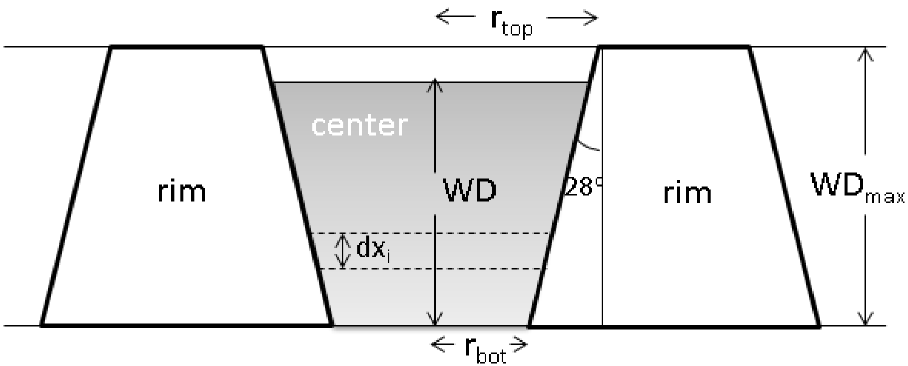

Fig. A2. Diagram of polygon rim and polygon center/lake, in which r_{top} is the radius of the top and r_{bot} that of the bottom of a polygon center or lake; WD and WD_{max} are the water depth, and maximum water depth in a polygon center or lake, respectively.

GMDD
6, 4883–4932, 2013